ACS Catalysis

Research Article

pubs.acs.org/acscatalysis

Cooperative Catalysis for Multistep Biomass Conversion with Sn/Al Beta Zeolite

Jan Dijkmans,[†] Michiel Dusselier,[†] Dries Gabriëls,[†] Kristof Houthoofd,[†] Pieter C. M. M. Magusin,[†] Shuigen Huang,[‡] Yiannis Pontikes,[‡] Maarten Trekels,[§] André Vantomme,[§] Lars Giebeler,[∥] Steffen Oswald,[∥] and Bert F. Sels*[,†]

[†]Center for Surface Science and Catalysis, KU Leuven, Kasteelpark Arenberg 23, 3001 Heverlee, Belgium

[‡]Department of Materials Engineering, KU Leuven, Kasteelpark Arenberg 44, 3001 Heverlee, Belgium

[§]Nuclear and Radiation Physics Section, KU Leuven, Celestijnenlaan 200D, 3001 Heverlee, Belgium

[∥]Institute for Complex Materials, Leibniz-Institute for Solid State and Material Research, Helmholtzstraβe 20, 01069 Dresden, Germany

Supporting Information

ABSTRACT: Lewis acid Snβ-type zeolites with varying amounts of Brønsted acid Al in the framework were synthesized using a simple two-step procedure comprising partial dealumination of β zeolite under action of acid, followed by grafting with $SnCl_4{\cdot}5H_2O$ in dry isopropanol. Characterization of the thus-prepared Al-containing Snβ (Sn/pDeAlβ) zeolites with ICP, (pyridine probed) FTIR, and ^{27}Al MAS NMR demonstrates the presence of Brønsted acid framework Al^{III}. Tetrahedral Lewis acidic Sn^{IV} is present, as ascertained by a combination of techniques such as EPMA, ^{119}Sn Möβbauer, XPS, (pyridine probed) FTIR, and UV−vis. A closed Sn^{IV} configuration was implied by comparing of ^{119}Sn solid-state MAS NMR and deuterated acetonitrile probed FTIR spectra with literature. The catalytic activity of the Al-containing Snβ was tested for the conversion of 1,3-dihydroxyacetone (DHA) into ethyl lactate (ELA), proceeding via pyruvic aldehyde (PAL). Despite the difference in synthesis between the classic hydrothermal Snβ reference and Sn/pDeAlβ, the activity of Sn for the Lewis acid-catalyzed hydride shift of PAL to ELA is similar. Yet, the overall reaction rate of DHA into ELA is faster with Sn/pDeAlβ because Brønsted acidity of the remaining framework Al^{III} facilitates the rate-determining dehydration of DHA into PAL. Materials containing moderate amounts of Al (0.3 wt % Al) show the highest ELA productivities, leading to a record value of 2113 g ELA·kg catalyst^{-1}·h^{-1} at 363 K. The cooperative effect of Lewis Sn^{IV} and Brønsted Al^{III} acid sites is verified by comparing catalytic data with physical mixtures of partially dealuminated β zeolite and Al-free Snβ.

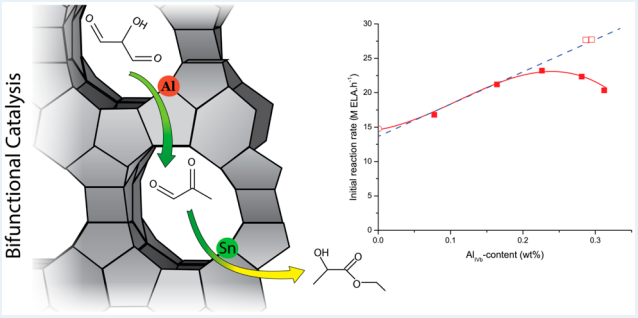

KEYWORDS: *heterogeneous catalysis, Snβ zeolite, postsynthesis procedure, bifunctional catalysis, Lewis acid catalysis, 1,3-dihydroxyacetone, ethyl lactate, biomass conversion*

The conversion of biomass—and mainly lignocellulose—into chemicals has been investigated intensely the past decade.[1] Next to the difficulty of selecting the proper target chemicals to synthesize from these renewable resources,[2] the search for suitable catalysts for their production is even more challenging and has led to interesting novel catalytic materials.[3] One such material, regularly recurring in this context, is Snβ zeolite.[1h,l,4] This zeolite is constructed of an ordered 3D network of SiO_2 tetrahedra with pores comprising 12 oxygen-bridged Si atoms but with Sn^{IV} occasionally substituting Si^{IV} in the framework. It shows high activity in relevant reactions such as sugar isomerization or epimerizations[4b,5] and the production of lactates from carbohydrates,[4c] as well as in more organic-oriented reactions like Baeyer−Villiger oxidation[6] and intermolecular Meerwein−Ponndorf−Verley reactions.[7] The presence of Sn introduces Lewis acidity into the β zeolite framework. Other porous materials have been functionalized with Sn^{IV} and tested for similar reactions,[8] but as long as the reactants are not too bulky, Snβ shows the highest activity. This property is attributed to its highly siliceous and crystalline nature, which is believed to create an internal hydrophobic material surface,[9] yielding a water-tolerant Lewis acid that proves to be very active, even in aqueous conditions.[4b,10]

The absence of trivalent T atoms like aluminum or boron results in a hydrophobic, hydrothermally stable and neutral framework without Brønsted acid sites.[11] Yet, a combination of Lewis and Brønsted acidity in such materials could play a beneficial role in several reactions from carbohydrates to

Received: September 15, 2014
Revised: December 2, 2014
Published: December 26, 2014

DOI: 10.1021/cs501388e
ACS Catal. 2015, 5, 928−940

chemicals. One exemplary cascade is the conversion of glucose, into 5-hydroxymethylfurfural (HMF). The Lewis acid sites catalyze glucose isomerization to fructose, while Brønsted acidity subsequently catalyzes its dehydration and conversion into HMF.[12] The lack of Brønsted acidity in Snβ has been overcome by adding mineral acids or by using a physical mixture with heterogeneous Brønsted acids. Davis et al., for instance, used a combination of Snβ and HCl to convert glucose into HMF using a biphasic solvent system. An organic phase was used to extract HMF and prevent rehydration and other side reactions.[13] For the same reaction, Tsapatsis et al. used Snβ in combination with HCl or Amberlyst resins. Stabilization of HMF was provided by esterification with ethanol, which also acted as solvent.[14] Lobo et al. applied Snβ in the same combination to yield furfural from xylose in a similar bifunctional catalytic reaction pathway.[15] Román-Leshkov et al. used a physical mixture of a Lewis acid Zrβ zeolite and Brønsted acid Al-MFI nanosheets, to convert furfural in a single reaction into γ-valerolactone in the presence of 2-butanol as hydride donor.[16] Recently, a first example of a single material containing both Lewis and Brønsted sites was reported in form of a Sn-containing highly oxygenated carbon-silica composite for direct conversion of sugars to lactate esters.[8e] Likewise, an Al-containing Snβ material was described for a conversion of cortalcerone to furylglycolic acid, but no information on its synthesis was given.[17]

Most previous examples with Snβ used additional reagents to combine Brønsted and Lewis acid sites, likely because the original recipe of Corma et al. omits Al^{III} in the synthesis gel, although Mal et al. reported a Snβ zeolite containing Al^{III} as early as 1997.[18] The classic synthesis of Al-free Snβ requires a long synthesis time and the necessity to use fluoride as mineralizing agent to effectively incorporate Sn^{IV} in framework positions. Seeding of the synthesis gels with dealuminated β seeds is now common practice to reduce the synthesis time drastically.[19] Several researchers nevertheless search for alternative synthesis procedures. One of the most recently reported pathways follows a complete dealumination of commercial β zeolites with a subsequent incorporation of Sn through grafting or solid-state ion exchange.[20] Using the former strategy, we recently reported a practical synthesis method to create Snβ-zeolites with exceptionally high activity in sugar isomerization. The materials were made by a two-step process, in which $SnCl_4{\cdot}5H_2O$ is grafted on an fully dealuminated commercial β-zeolite from an alcohol solution.[4a]

Herein we report the synthesis and physicochemical characterization of a Snβ zeolite, incorporating both Brønsted and Lewis acid sites by using partially dealuminated commercial β zeolite in the grafting procedure, according to Scheme 1. The bifunctional catalytic properties of the Al-containing Snβ is demonstrated in the one-step conversion of trioses to ethyl lactate in ethanol. This conversion includes both a dehydration and a hydride shift, which are catalyzed by Brønsted and Lewis acid sites, respectively.[8e] The catalytic results will prove a beneficial cooperative effect of the active sites for the chosen reaction.

EXPERIMENTAL SECTION

Material Synthesis. The catalytic materials were synthesized by adapting a previously described method.[4a] Commercial β zeolite (CP814e, Zeolyst International, SiO_2/Al_2O_3 = 25) was dealuminated by stirring the zeolite powder in an aqueous HNO_3 solution (55 mL per gram of zeolite, at 353 K overnight), the acid concentration varying in the range 1.44–14.4 M, depending on the desired degree of Al^{III} removal. Afterward the powders were filtered, washed with water, and dried at 333 K. Before grafting, the powders were dried at 423 K to remove excess of physisorbed water. Dealuminated zeolite was added to $SnCl_4.5H_2O$ (27 mmol/g of zeolite) in dried isopropanol (100 mL/g of zeolite) and placed in a reflux setup under N_2 atmosphere. After 7 h, the mixture was filtered in air, rinsed with dry isopropanol, dried at 333 K, and calcined (3 K/min to 473 K, dwell 6 h, 3 K/min to 823 K, dwell 6 h). A sample with an elevated Sn content was synthesized by using a higher $SnCl_4{\cdot}5H_2O$ concentration (45 mmol/g of zeolite, double the normal concentration). Samples are labeled as Sn/XpDeAlβ, in which X represents the molarity in HNO_3 used in the partial dealumination (pDeAl) step. The sample grafted with higher Sn concentration is denoted with 2×Sn/XpDeAlβ. Alβ represents the Al-containing parent zeolite.

Scheme 1. Schematical Representation of the Synthesis of the Materials[a]

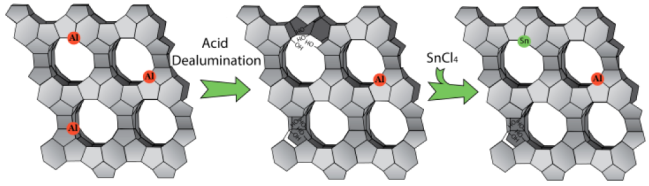

[a]A commercially available β zeolite is partially dealuminated by acidic treatment in aqueous HNO_3, followed by contact with $SnCl_4{\cdot}5H_2O$ in dry isopropanol. Eventually, a β zeolite containing both Sn^{IV} (Lewis acid sites) and Al^{III} (Brønsted acid sites) is obtained.

Material Characterization. Elemental analyses of Al were performed on a PerkinElmer Optima DV 3300 ICP-AES at 396.2 nm, after dissolving the solid samples in 1 M NaOH, further diluted and acidified with HNO_3 before measurement. The Sn content of the materials were determined by electron probe microanalyzer (EPMA) analysis conducted on a JEOL JXA-8530F field emission microprobe using WDS. Samples were embedded in a resin, the surface was ground, polished, and coated with carbon before measurement. The microprobe was operated at 10 kV with a probe current of 1.5 nA. The Sn $L_{\alpha 1}$-signal was detected using a PETH crystal, and the Sn concentration was quantified with a cassiterite standard. ZAF (Z: Atomic number correction, A: Absorption correction, F: Characteristic fluorescence correction) was used for the matrix correction method. XPS experiments were performed on a Physical Electronics PHI 5600 CI with Mg Kα (1253.6 eV) radiation in an energy range of 0–1000 eV. The spectrometer was equipped with a hemispherical analyzer allowing high sensitivity and high-resolution experiments. Energy scale and binding energy were calibrated with Cu, Ag, and Au foils at the binding energies of Cu $2p_{3/2}$ (932.67 eV), Ag $3d_{5/2}$ (368.26 eV), and Au $4f_{7/2}$ (84.00 eV), respectively. The sample chamber was held at a pressure of 10^{-9} to 10^{-10} mbar. High-resolution spectra were taken with a pass energy of 29 eV and a step size of 0.1 eV. All spectra were normalized to Si $2p_{3/2}$ = 103.6 eV. All spectra are Shirley background corrected and satellite subtracted. FT-IR measurements were performed on a Nicolet 6700 Spectrometer equipped with DTGS detector. Calcined samples were pressed into self-supporting wafers and degassed at 673 K in vacuo in situ before measurements. Lewis acid sites were analyzed by using pyridine and deuterated acetonitrile probes. For pyridine adsorption, the samples were subjected to

DOI: 10.1021/cs501388e
ACS Catal. 2015, 5, 928–940

Table 1. Physicochemical Properties of the Synthesized Materials[a]

entry	sample	dealumination strength [M]	Al content[b] wt % (Si/Al)	Sn content[c] wt% (Si/Sn)	Brønsted acidity[d] μmol acid·g^{-1}	Lewis acidity[d] μmol acid·g^{-1}
1	Alβ	/	2.76 (15)	0	/	/
2	7.2pDeAlβ	7.2	0.28 (160)	0	/	/
3	Sn/14.4pDeAlβ	14.4	0.10 (440)	1.65 (116)	16	83
4	Sn/7.2pDeAlβ	7.2	0.21 (209)	1.57 (122)	23	88
5	Sn/3.6pDeAlβ	3.6	0.29 (151)	1.59 (121)	31	83
6	Sn/2.88pDeAlβ	2.88	0.37 (119)	1.45 (132)	54	77
7	Sn/1.44pDeAlβ	1.44	0.48 (91)	1.51 (127)	82	78
8	2×Sn/2.16pDeAlβ	2.16	0.42 (101)	3.58 (52)	62	138
9	2×Sn/1.8pDeAlβ	1.8	0.40 (111)	3.70 (50)	62	153
10	Snβ[e]	/	0 (∞)	1.58 (122)	3	78

[a]Samples were calcined and hydrated. Samples are labeled as Sn/XpDeAlβ, in which X represents the molarity in HNO_3, used in the partial dealumination (pDeAl) step. 2×Sn indicates the use of a higher Sn concentration during the grafting procedure. [b]Determined by ICP-OES. Values in brackets are molar ratios. [c]Determined by EPMA-analysis. Values in brackets are molar ratios. [d]Determined by pyridine-probed FTIR. [e]Snβ in entry 10 is the classic hydrothermal Snβ.

25 mbar of the probe until saturation at 323 K. Spectra were recorded at 423 K in vacuo after equilibration for 20 min. 1.02 and 0.89 cm.μmol^{-1} were used as integrated molar extinction coefficients for calculations of Brønsted and Lewis acid density, respectively.[21] Deuterated acetonitrile was adsorbed at room temperature. The samples were exposed to 100 mbar of probe molecule for 10 min, afterward desorption in vacuo of the molecule was followed at the same temperature. For both probe molecules, spectra of unloaded materials were recorded as reference spectra. Diffuse reflectance measurements in the UV−vis region were recorded on an Agilent Cary 5000 spectrophotometer. Samples were placed in a quartz tube with window and were dried at 823 K before measurement, if indicated. X-ray diffraction patterns were recorded on a STOE Stadi P diffractometer equipped with Cu- $K\alpha_1$ source and IP-PSD detector. Before measurement, the samples were stored in a humidity controlled environment, that is, above a saturated NH_4Cl solution (79% humidity). Measurements were carried out in 1 mm Hilgenbergglass capillaries. Mößbauer spectroscopy were measured in transmission geometry, using a gas proportional counter at 23.88 keV nuclear resonance. Nominal activity of the ^{119m}Sn source was 370 MBq (Matrix $CaSnO_3$). The line width of the radiation emitted from the source was determined to be 0.75 ± 0.01 mm/s fwhm. Measurements of the samples and standard materials like SnO_2, SnO, and Sn^0 were performed at room temperature. A Lorentzian line shape model was used to fit the results. ^{27}Al and ^{119}Sn MAS NMR spectra were recorded on a Bruker DSX400 spectrometer (B_0 = 9.4 T) operating at a ^{27}Al NMR frequency of 104.26 MHz and a ^{119}Sn NMR frequency of 149.21 MHz. For ^{27}Al MAS NMR, single-pulse excitation was employed with a strong pulse of 0.3 μs (278 kHz nutation frequency), and 36 000 scans were accumulated with a recycle delay of 100 ms. The samples were packed in 2.5 mm rotors after hydration and rotated at a spinning frequency of 20 kHz. A 0.1 M aqueous solution of $Al(NO_3)_3{\cdot}9H_2O$ was used as chemical shift reference. For ^{119}Sn MAS NMR, single-pulse excitation with and without proton decoupling and varying interscan delays between 5 and 40 s have been used. A total of 26 992 scans were accumulated. The samples were packed in 4 mm zirconia rotor (for the dried samples this was done in an 80/20% v/v Ar/O_2 environment, to shorten the T1-relaxation time); the spinning frequency of the rotor was 12 kHz. The chemical shift is referenced with respect to $Sn(CH_3)_4$. SnO_2 was used as a secondary standard; the chemical shift of its center band was set at −604.0 ppm.[22] ^{29}Si MAS NMR spectra were recorded on a Bruker AMX300 spectrometer (B_0 = 7.0 T) equipped with a 4 mm MAS probe head. At this field, the resonance frequency of ^{29}Si is 59.6 MHz. 5400 scans were accumulated with a recycle delay of 10 s. The sample-rotation rate was 3 kHz. Tetramethylsilane was used as chemical shift reference. SEM pictures of the samples were taken with a Philips XL 30 FEG, and samples were coated with gold prior to measurement.

Catalytic Tests. Catalytic tests were performed in magnetically stirred and closed glass reactors of 10 mL, which were placed in a copper block, heated at 363 K. Temperature control is carried out in a reference glass reactor with solvent. Seventy-five milligrams of catalyst was added to 1 mmol of substrate in 5 mL of ethanol, and 1,4-dioxane was used as the internal standard for chromatographic analysis. For competitive homogeneous reactions, 5 mol % of $SnCl_4{\cdot}5H_2O$ was added to 1 mmol of each substrate, whereas other parameters were kept similar to the heterogeneously catalyzed reactions. Aliquots of sample were taken at regular time intervals through a rubber septum and were quantitatively analyzed with an Agilent 6850 GC, equipped with a HP-1 column and FID detector for the volatile products. Identification of these products was based on retention time analysis and confirmed by GC-MS (Agilent 6890 GC with HP5-MS column and Agilent 5973 Mass Selective Detector). The nonvolatile products like sugars were analyzed with an Agilent 1200 series HPLC equipped with Aminex 87C column and a refractive index detector. Quantification was done by calibrations with standard solutions.

RESULTS AND DISCUSSION

We recently described a practical procedure for grafting Sn^{IV} on fully dealuminated β zeolite,[4a] which we here extend to produce Sn^{IV} grafted on partially dealuminated β samples, denoted as Sn/pDeAlβ. In short, the partial dealumination of commercial Alβ zeolite induces the formation of a silanol nest at the site where Al^{III} is removed. Subsequent grafting with $SnCl_4{\cdot}5H_2O$, dissolved in dry isopropanol, results in a zeolite, where Sn sites are anchored on the Si−OH groups. In what follows, the Sn/pDeAlβ zeolites are characterized with main focus on their Lewis and Brønsted acid properties. Next, the bifunctional catalytic superiority of the Sn/pDeAlβ zeolites will be demonstrated, with a focus on the cooperative effect of the

DOI: 10.1021/cs501388e
ACS Catal. 2015, 5, 928−940

two acid sites in the conversion of trioses to ethyl lactate in ethanol. The choice of the reaction is corroborated by the increasing importance of the chemical synthesis of lactic acid and its esters, as a promising renewable platform chemical.[2d,e,23]

Synthesis and Compositional Aspects of Sn-Grafted Al*β* Zeolites. Procedures for zeolite dealumination are well documented in literature.[24] Complete removal of Al from the zeolite *β* framework for instance requires a 20 h acidic treatment with 13 M HNO_3 at 373 K. Partial dealumination of zeolite *β* was therefore achieved at lower acid concentrations, contact time, and dealumination temperature. Here, the commercial Al*β* zeolite (Table 1, entry 1) was subjected to an acid treatment overnight with varying HNO_3 concentrations ranging from 1.44 to 14.4 M at 353 K. The elemental analysis in Table 1 clearly shows increasing Al^{III} removal with increasing proton concentration in the acid treatment (compare entries 3 to 7, Table 1). For instance, a Si/Al ratio of 440 was measured for samples contacted with 14.4 M HNO_3 , this ratio was 91 when treated with 1.44 M HNO_3. Except for entry 8 and 9, all materials were grafted using identical solutions of $SnCl_4.5H_2O$ in isopropanol (0.27 M), followed by a drying step at 473 K prior to calcination at 823 K, following a procedure described elsewhere.[4a,25] The amount of Sn is very similar for all samples and equals 1.6 wt % (compare entries 3 to 7, Table 1). Higher Sn loadings, viz., 3.6 wt %, were obtained by increasing the $SnCl_4$ concentration in isopropanol (entries 8 and 9, Table 1). Note that the grafting procedure slightly reduces the Al^{III} content further due to additional dealumination activity during Sn grafting likely the consequence of HCl formation. For instance, a partially dealumination of a sample using 7.2 M HNO_3 results in a material with an atomic Si/Al ratio of 160, which further increases to 209 after grafting with $SnCl_4$ (compare entries 2 and 4, Table 1).

Structural and Spectroscopic Characteristics of the Sn-Grafted pDeAl*β* Zeolites. Diffraction patterns of various Sn-grafted dealuminated materials, displayed in Figure S1, show reflection patterns identical to that of the parent *β* zeolite in all cases. The broad nature of the signals, in comparison with the hydrothermally synthesized Sn*β*, is due to the smaller size of the particles of the used parent material (10−30 nm, as measured with SEM vs 1000−1500 nm (Figure S3)).[4a,26] No reflections of crystalline SnO_2 were found in the samples, which is obviously due to the low Sn content; note that the detection limit in XRD is about 0.5 wt % of crystalline SnO_2, physically mixed with commercial Al-containing *β* zeolite (see Figure S2). The result of a ^{119}Sn Mö*β*bauer spectroscopic analysis is illustrated in Figure S4 for the Sn/7.2pDeAl*β* sample. A signal with an Isomer Shift (IS) of −0.24 mm·s^{-1} and Quadrupole Splitting (QS) of 0.50 mm·s^{-1} was recorded, which accords to a Sn^{IV} species, highly coordinated by oxygen. No hints on reduced oxidation states of Sn, such as Sn^0 and Sn^{II}, are found in the spectrum. The presence of Sn° should give a singlet at 2.69 mm·s^{-1} (QS 0 mm·s^{-1}), while oxygen-coordinated Sn^{II} should show a doublet centered around 2.80 mm·s^{-1} with QS of 1.46 mm·s^{-1}.[27] Shift and splitting are similar to earlier reported ^{119}Sn Mö*β*bauer data of Sn^{IV}-MFI zeolites.[28] No observable intensities of signal shifts attributed to SnO_2 (IS 0.12 mm·s^{-1} and QS 0.03 mm·s^{-1}) and $SnO_{4-x}Cl_x$ (IS 0.42 mm·s^{-1} and QS 0.41 mm·s^{-1}) species (unreacted and partially reacted $SnCl_4$) were found. Mö*β*bauer detection limits of 0.27 and 0.11 wt % Sn, coexisting as SnO_2 and $SnCl_4$, respectively, in the 1.6 wt % Sn/pDeAl*β* samples were obtained by modeling (see Supporting Information, Figures S4−S6). Photoelectron spectroscopy data (XPS) of the Sn/pDeAl*β* material is depicted in Figure 1a. No signs of Sn−Cl bonds were retrieved from the

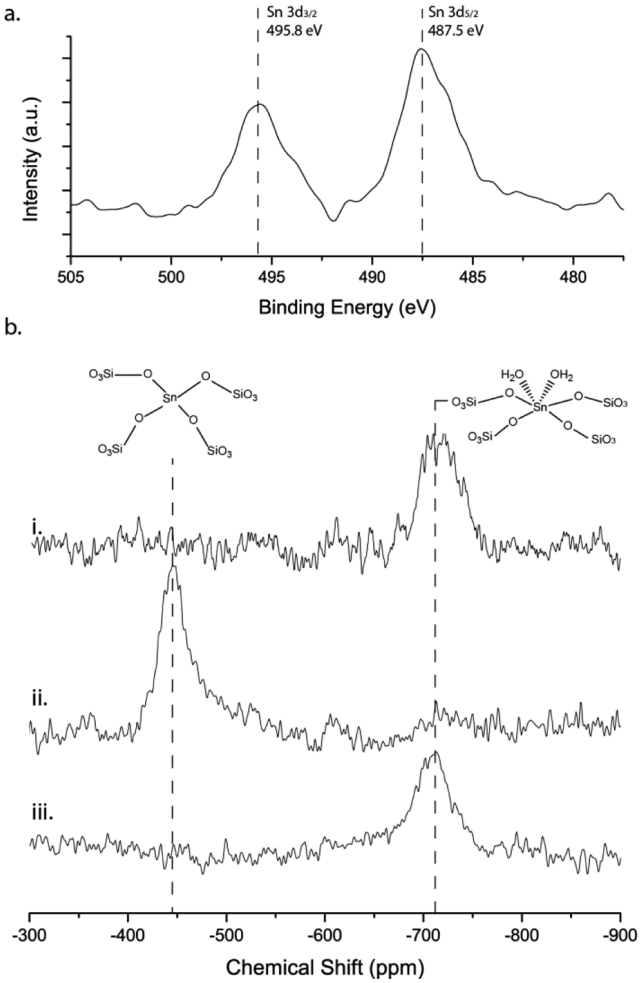

Figure 1. (a) Sn 3d XPS spectra of Sn/7.2pDeAl*β*. (b) ^{119}Sn MAS NMR spectra of (i) hydrated, (ii) dehydrated, and (iii) rehydrated Sn/7.2pDeAl*β* (1.5 wt % Sn, natural abundance ^{119}Sn). Dehydration of the sample occurred in a dry N_2-flow at 573 K, rehydration was accomplished by opening the NMR rotor and exposing the dried sample of (b) to atmosphere for 6 h. Structures on top display corresponding species as assigned in literature.

data, supporting the Mö*β*bauer results in the claim that no partially reacted SnO_xCl_{4-x} species remain in the Sn/pDeAl*β* sample. The spectra display signals of the Sn $3d_{3/2}$ and $3d_{5/2}$ binding energies (BE) at 495.8 and 487.5 eV, indicative of Sn^{IV} and similar to BE reported in literature for Sn*β* materials.[5b]

Sn^{IV} should preferentially be present in tetrahedral coordination (when in dry form), and not in octahedral coordination like in SnO_2, as the latter shows poor catalytic activities.[29] No signals typical for SnO_2 (−604 ppm) and $SnO_{4-x}Cl_x$ ($SnCl_4$: −150 ppm) species were retrieved by ^{119}Sn MAS NMR (performed on non-^{119}Sn-enriched sample), in agreement with Mö*β*bauer and XPS results (a detection limit test for bulk SnO_2 is presented in Supporting Information). A representative result of the ^{119}Sn MAS NMR measurements is illustrated in Figure 1b (i) for sample Sn/7.2pDeAl*β*. The spectrum of the hydrated sample shows a broad signal at −711 ppm, which is indicative of a Sn^{IV} single site, coordinated with water ligands. This chemical shift is slightly different than

DOI: 10.1021/cs501388e
ACS Catal. 2015, 5, 928−940

recently reported shifts for hydrothermal Snβ (−700 ppm),[29,30] but chemical shifts from -654 ppm up to −736 ppm have been reported for hydrated Snβ.[6,31] Drying of the sample in N_2 at 573 K, prior to the NMR experiment, causes a complete shift of the −711 ppm signal toward −445 ppm (Figure 1b (ii)). Recent papers assigned this signal to the closed, tetragonal Sn^{IV} in the β framework, viz., $Sn^{IV}(OSi)_4$. The open form, $Sn^{IV}(OSi)_3(OH)$, was proposed to be located at around −420 ppm, .[29,30,32] No clear signal of the latter was found for the Sn/pDeAlβ samples of this study. Exposing the dried sample to humid air causes the Sn site to rehydrate, which was confirmed by reversible reappearance of the −711 and disappearance −445 ppm chemical shifts in Figure 1b (iii). The presence of a closed Sn site in the β framework seems to be confirmed by a d_3-acetonitrile FTIR sorption measurement, shown in Figure 2. A clear signal at 2310 cm^{-1} was observed for

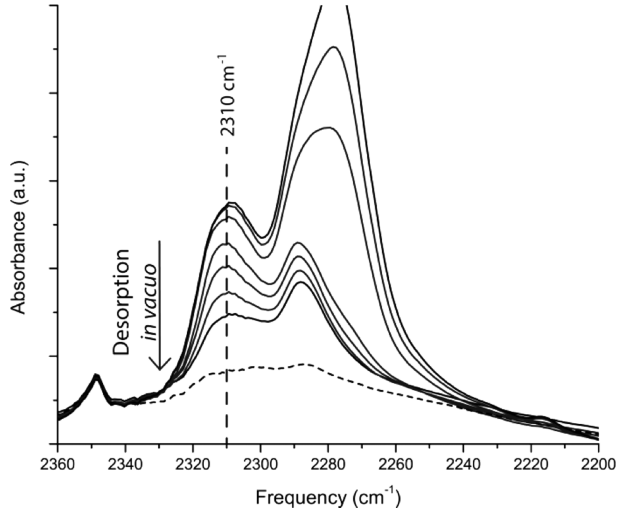

Figure 2. FTIR spectra of Sn/7.2pDeAlβ (dotted line) and adsorbed deuterated acetonitrile (full lines) at different stages of desorbing in vacuo.

chemisorbed CD_3CN. The observed frequency resembled this of closed Sn sites, as was assigned by Boronat et al. (2308 cm^{-1}), whereas no signal was detected for open Sn sites, located at 2316 cm^{-1}.[33] Signals of acetonitrile sorbed onto Brønsted acid sites (around 2290 cm^{-1}) and acetonitrile sorbed onto silanol groups (2274 cm^{-1}) are also present.[34] Similar to literature, the spectrum of CD_3CN adsorbed onto the hydrothermal Snβ showed the presence of closed sites, with the main signal around 2308 cm^{-1} (see Figure S9). UV−vis Diffuse Reflectance Spectroscopy (DRS) of the Sn/Alβ zeolites in hydrated and dry state were measured, and the representative spectra are shown in Figure 3. The electronic absorption spectrum of the hydrated Al-containing Snβ (spectrum a) shows a broad but less intense absorbance around 270 nm and one sharper at 220 nm. The latter is usually attributed to tetrahedrally coordinated Sn^{IV}, the former has been typically assigned to octahedral Sn^{IV}, either as an extra-framework SnO_2 phase or as double hydrated framework Sn^{IV} single-site species.[4a] Because absence of SnO_2 was hinted with ^{119}Sn MAS NMR and Möβbauer and drying of the sample caused a disappearance of the signal (spectrum in Figure 3b), the 270 nm absorption is attributed to hydrated Sn^{IV}. UV−vis is fairly sensitive in detecting SnO_2 phases: the detection limit of octahedrally coordinated Sn^{IV}, such as in SnO_2 phases, is less

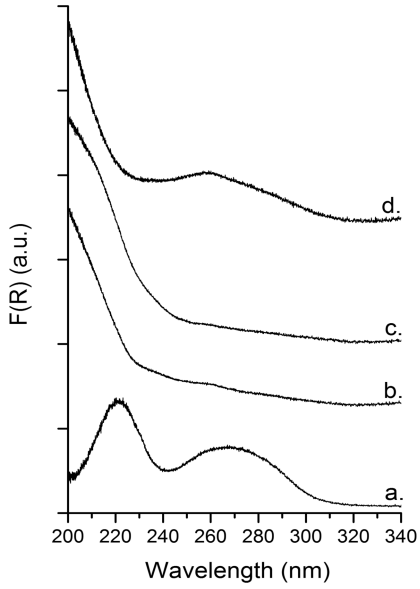

Figure 3. UV−vis DR spectra of (a) hydrated Sn/7.2pDeAlβ and dehydrated (b) Sn/7.2DeAlβ, (c) Sn/1.44DeAlβ, and (d) 2×Sn/2.16pDeAlβ. Drying of the samples was performed at 573 K in a dry N_2 flow. All samples are corrected with their respective pDeAlβ spectrum.

than 0.08 wt % Sn in the powder sample (see Figure S10 and S11). Upon drying, the 220 nm tetrahedral Sn^{IV} signal slightly shifts to lower wavelengths, as was observed earlier.[4a] Presence of varying amounts of Al has no real influence on the coordination of Sn as the electronic spectra of all dehydrated samples displayed virtually identical patterns. A representative sample with more aluminum is shown in Figure 3c (spectra of all materials with varying Al-content are shown in Figure S12). The UV−vis spectrum of a dehydrated 2×Sn/2.16pDeAlβ, a material with a much higher Sn content (Table 1, entry 8), shows a broad signal around 260 nm in Figure 3d, which is attributed to octahedral extraframework SnO_2. Such high Sn loadings should thus be avoided. As a comparison, also the electronic absorption spectrum of the hydrothermally synthesized Snβ standard material is displayed in Figure S12. The sample shows absorption characteristics similar to those described in literature for similar materials:[29] a maximum intensity at 215 nm, assumed to be isolated tetrahedral Sn^{IV}, and a shoulder expanding to 300 nm.

The partial removal of Al upon acid treatment, as reported in the elemental analysis in Table 1, is also evident from FTIR. IR spectra of the 3400 to 3800 cm^{-1} region are displayed in Figure 4. Effects of the dealumination are visible in spectra a−f. The data show a consistent intensity decrease of vibrations at 3610, 3670, and 3780 cm^{-1}, resulting from O_3Si−O(-H)-AlO_3, perturbed and unperturbed AlO-H species, respectively,[24,35] with increasing Al removal. Although the vibration of acidic Si−O(-H)-Al sites at 3610 cm^{-1} remain visible after treatment with diluted HNO_3 solutions, the signal disappears in the broad tail of hydrogen bonded Si−OH groups, ranging from 3600 to 3300 cm^{-1}, for the more severely dealuminated samples. Changes in the presence and identity of silanols can also be observed. While the original Alβ zeolite shows the presence of some external silanols at 3740 cm^{-1}, an intense and broader vibrational signal at 3730 cm^{-1} appears in the spectra of the partially dealuminated Sn/pDeAlβ zeolites. This signal is attributed to silanol nests, resulting from excessive removal of

DOI: 10.1021/cs501388e
ACS Catal. 2015, 5, 928−940

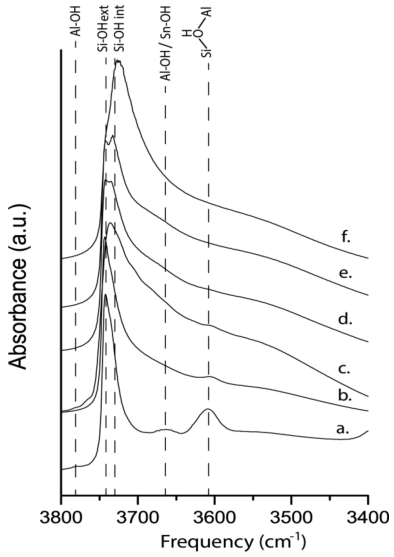

Figure 4. FTIR of the silanol region of (a) Alβ, (b) Sn/1.44pDeAlβ, (c) Sn/2.88pDeAlβ, (d) Sn/3.6pDeAlβ, (e) Sn/7.2pDeAlβ, and (f) Sn/14.4pDeAlβ. Signals are scaled to weight.

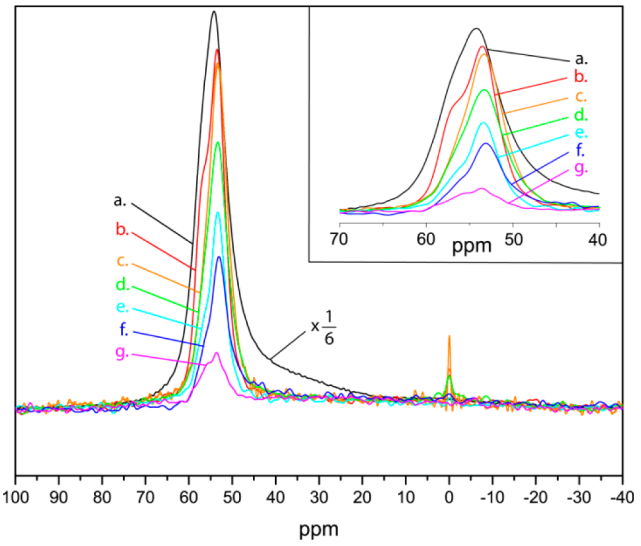

Figure 5. ^{27}Al MAS NMR of the materials (a) Alβ, (b) Sn/1.44pDeAlβ, (c) Sn/1.8pDeAlβ, (d) Sn/2.88pDeAlβ, (e) Sn/3.6pDeAlβ, (f) Sn/7.2pDeAlβ, and (g) Sn/14.4pDeAlβ. The inset shows a close-up of the tetrahedral Al region. Samples contain 0.10−0.40 wt % of Al for the dealuminated samples. Signals are scaled to weight.

Al^{III},[24b,36] and this signal is indeed more intense in samples with lower Al^{III} contents. Its presence shows that not all internal SiOH groups in the Sn/pDeAlβ zeolites are saturated with Sn^{IV}, and thus the final structure contains residual "holes". The presence of remaining silanol groups in fully dealuminated materials synthesized with the same two-step technique has been demonstrated with solid-state ^{29}Si MAS NMR in a previous publication.[4a] The ^{29}Si MAS NMR spectra of a Sn/pDeAlβ sample are presented in Figure S13, showing a signal at −102 ppm, which is attributed to the presence of $(SiO)_3SiOH$. No such silanol signals were found for the hydrothermally synthesized Snβ standard material, indicating a difference in hydrophobicity between both materials. A weak shoulder at 3665 cm^{-1} is also present in the Sn/pDeAlβ zeolites, which we tentatively attribute to the presence of Sn−OH species, in accordance with similar vibrations of Sn species on the surface of SiO_2, as reported earlier.[4a,37]

In the ^{27}Al MAS NMR, found in Figure 5, the overall signal intensities (which are scaled to weight) drop upon dealumination. The spectra of the Sn/pDeAlβ samples and the original Alβ zeolite show an intense signal in the 50−60 ppm region, corresponding to tetrahedrally coordinated Al_{IV}, typically associated with the Brønsted acidity of zeolites. The parent Sn-free Alβ zeolite also exhibits the octahedrally coordinated Al_{VI} signal at 0 ppm, but the signal intensity is low, and broadens with increasing acid concentration. A similar trend was observed in Zn-exchanged beta zeolites.[38] Detailed investigation of the tetrahedral Al_{IV} (inset Figure 5) shows that the broad line width of the signal can be attributed to the presence of different Al_{IV} sites. The spectra reveal the presence of at least two signals, Al_{IVa} around 57 ppm and Al_{IVb} at 54 ppm. Literature reports that Al_{IVa} could be attributed to partially hydrolyzed Al species such as $(SiO)_3AlOH$ at surfaces and defects in the crystal lattice, whereas Al_{IVb} could be assigned to framework Al species.[39] Other reports attribute the different signals to Al atoms at different crystallographic positions in the zeolite framework.[39a,40] Recently, it was shown that Al sites at specific crystallographic positions show individual behavior toward dealumination; some are removed more easily, although others seem more resilient toward removal.[40] Though all NMR signals ultimately decrease with increasing dealumination harshness, a clear asymmetry is observed confirming the different acid sensitivity of the Al_{IV}-species, in accordance with literature.[24b,39a]

The Brønsted and Lewis acidity of the hydrothermal β zeolites and the various Sn/pDeAl-containing β zeolites are probed with FTIR spectroscopy after pyridine adsorption. The pyridine spectra show characteristic vibrations of Brønsted acid sites at 1540 cm^{-1} and Lewis acid sites at 1450 cm^{-1}, illustrating the bifunctional nature of the Sn/pDeAlβ materials. Results of quantitative measurements of both acid types are found in Table 1, for which the extinction factors, as described by Nesterenko et al. (1.02 and 0.89 cm·μmol^{-1} for Brønsted and Lewis acid sites, respectively), were used.[21] Assuming one pyridine molecule adsorbing per Sn, a Lewis acid concentration of 130 μmol·g^{-1} for 1.5 wt % Sn is expected, but lower acid concentrations were measured (around 80 μmol·g^{-1} or about 62% of the theoretical maximum). Nevertheless, no higher adsorbed pyridine surface concentrations were measured upon extended exposure to higher pyridine pressure or multiple dosing of the probe molecule. Measurements performed at lower temperatures (<423 K) were hampered by the presence of physisorbed pyridine, making correct quantification impossible (due to overlap of a broad signal at 1445 cm^{-1} for hydrogen bonded pyridine and the 1450 cm^{-1} signal for Lewis acid bonded pyridine). The mismatch of the theoretical and measured concentration may indicate a limited accessibility of the acid sites for pyridine probing, or the presence of very weak Lewis acid sites of which the probe molecule desorbs at temperatures below the analysis temperature of 423 K, but it may well be the result of the usage of a wrong molar extinction coefficient in the quantification, as several different values have been proposed in literature.[21,35,41] Similar effects have been reported for other zeolites in literature.[21] Limited accessibility leading to a reduced catalytic efficiency in Snβ zeolites, even for small molecules, was very recently demonstrated in large crystals[42] and thus may realistically contribute to the under-

DOI: 10.1021/cs501388e
ACS Catal. 2015, 5, 928−940

estimate of the acid site density, as obtained by the sorption of the larger pyridine molecule. Doubling the Sn content in Sn/pDeAlβ does not result in twice the number of Lewis acid sites (compare entries 7 and 8). This behavior is in concert with the presence of some non-Lewis acid SnO_2 phases, in agreement with the electronic absorption spectrum of the high Sn loadings (sample 2×Sn/2.16pDeAlβ, see UV−vis data in Figure 3). The 1540 cm^{-1} signal, linked to Brønsted acid sites, is virtually absent in the hydrothermal Snβ zeolite. For the Sn/pDeAlβ materials, the observed Brønsted acidity is significantly lower than the Al content, which can be attributed to (i), another case of limited pyridine accessibility or underestimate of the molar extinction coefficient, or (ii), by the presence of non-Brønsted acidic Al species. Assuming an accessibility of 62% (derived from the Lewis acid sites, vide supra), we found the concentration of Brønsted acid sites to correspond best to the amount of Al_{IVb} in the zeolite samples, as presented in the acidity site summary plot seen in Figure 6 (calculations on Al_{IVa} and Al_{IVb} concentrations and plots correlating Al_{IVa} and Al_{IVa}+Al_{IVb} versus Brønsted acid concentration can be found in Figure S14 and S15), suggesting that mainly Al_{IVb} sites, which are distinctively detected in ^{27}Al MAS NMR, have Brønsted acid properties. This property is in line with results published in literature for the identity of Al_{IVa} and Al_{IVb} to be partially hydrolyzed (nonacidic) Al_{IV} species and Brønsted acid framework Al_{IV} species, respectively.[39b]

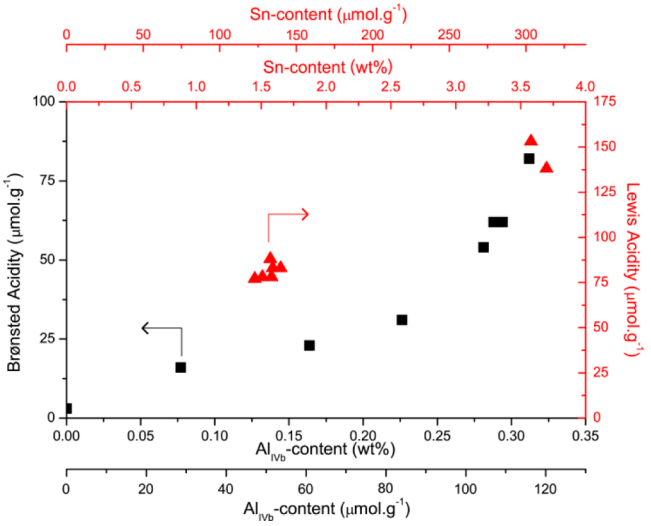

Figure 6. Plot of Brønsted and Lewis acidity per weight of material, obtained with quantitative FTIR probed pyridine sorption, in function of the Al_{IVb} (bottom) and Sn content (top) of the materials, obtained by ICP and EPMA analysis, respectively.

In conclusion, the synthesized Sn/pDeAlβ zeolites have a BEA topology and Sn is exclusively present in oxidation state IV, which was confirmed by ^{119}Sn Möβbauer and XPS measurements. UV−vis DRS and ^{119}Sn MAS NMR indicate a tetrahedral Sn coordination, and no significant amount of SnO_2 was detected, unless an elevated Sn loading was used (3.6 wt %). Comparison of ^{119}Sn MAS NMR and FTIR of sorbed deuterated acetonitrile with literature points to a closed Sn site. The custom Sn/pDeAlβ zeolites contain considerable quantities of tetrahedral Al, its content depending on the HNO_3 concentration during the dealumination treatment. These sites are not present in hydrothermal Snβ. The tetrahedral Al is partly located in the framework and partly at external surfaces. The framework species generate Brønsted acid catalytic sites.

Catalytic Property of Sn-Grafted pDeAlβ Zeolites. Many catalytic reactions with sugar molecules require a combination of both Brønsted and Lewis acid catalytic sites. Conversion of glucose and xylose to HMF[13] and furfuraldehyde,[15,43] respectively, are intensely studied, next to the conversion of sugars such as sucrose, glucose, and trioses to lactic acid and alkyl lactates.[2d,4c,8e,44] More recently, we reported the conversion of glycolaldehyde and tetroses to vinyl glycolate and α-hydroxybutyrate esters,[23a,45] and Yamaguchi et al. reported on the conversion of formaldehyde with 1,3-dihydroxyacetone to α-hydroxy-γ-butyrolactone and lactic acid.[46] These reactions also benefit from the simultaneous presence of both acid types.

To demonstrate the effectivity of having both acid types in the Sn/pDeAlβ zeolites, the conversion of 1,3-dihydroxyacetone (DHA) into ethyl lactate (ELA), which is useful as a green solvent and in the polymer industry,[47] was investigated in ethanol. The reaction network has been studied intensively,[8e,f,48] and there is a general agreement that DHA, in fast equilibrium with its isomer glyceraldehyde (GA), undergoes dehydration and rearrangement into pyruvic aldehyde (PAL) (Scheme 2). This reaction is catalyzed by Lewis acid and Brønsted acid sites. In presence of an alcohol and Brønsted acid catalytic sites, PAL can be reversibly converted into the hemiacetal pyruvic aldehyde ethyl hemiacetal (PAEA), yet too strong Brønsted acid sites should be avoided because of pyruvic aldehyde diethyl acetal (PADA) formation. Lewis acid sites further convert the PAEA into ELA by means of a hydride shift.

Scheme 2. Overview of the Reaction Pathways[a]

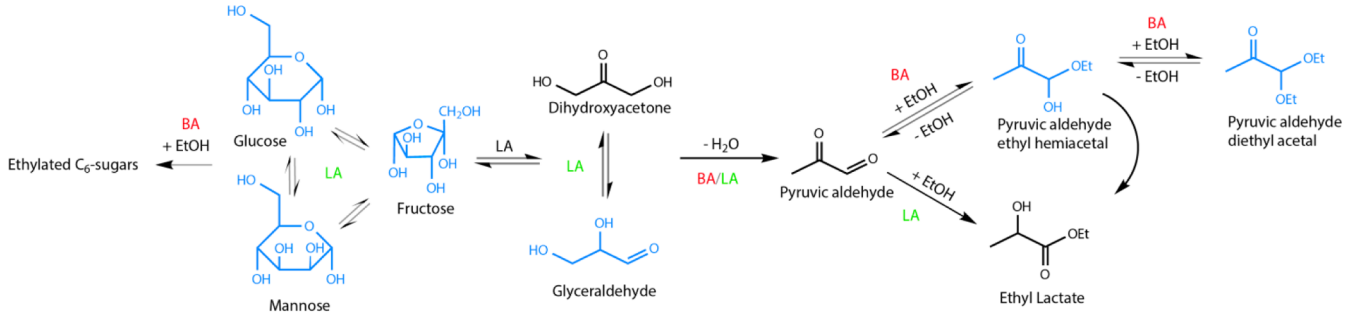

[a]The catalytic site needed for each reaction is displayed for each reaction (Brønsted acid site (BA) is red, Lewis acid site (LA) is green). The main reaction of dihydroxyacetone to ethyl lactate is pictured in black, and products of the side reaction are displayed in blue.

DOI: 10.1021/cs501388e
ACS Catal. 2015, 5, 928−940

Table 2. Results of Catalytic Tests with PAL[a]

entry	sample	ELA yield[b] %	productivity[b] $g_{ELA}\cdot kg_{catalyst}^{-1}\cdot h^{-1}$	TOF Sn[b] $mol_{ELA}\cdot mol_{Sn}^{-1}\cdot h^{-1}$	final yield/selectivity[c] %
1	Alβ	7	448	/	n.a.
2	7.2pDeAlβ	7	437	/	n.a.
3	Snβ	72	4523	286	>99
4	Sn/14.4pDeAlβ	71	4453	270	>99
5	Sn/7.2pDeAlβ	70	4411	281	>99
6	Sn/3.6pDeAlβ	69	4373	275	>99
7	Sn/2.88pDeAlβ	67	4240	283	>99
8	Sn/1.44pDeAlβ	67	4187	277	>99
9	2×Sn/2.16pDeAlβ	77	4839	139	>99
10[d]	Sn/3.6pDeAlβ	29[d]	2354	173	44
11[e]	Sn/3.6pDeAlβ	25[e]	3540	148	98
12[d]	Snβ[f]	31[d]	2530	195	97
13[e]	Snβ[f]	10[e]	1381	60	82

[a]Catalyst (50 mg) was added to 1 mmol of PAL in 5 mL of ethanol. Reactions were conducted at 363 K. [b]TOF = turnover frequency. Based on samples taken after 15 min of reaction. [c]Final yield and selectivity after 6 h of reaction. [d]Reaction with glyoxal, product is ethyl glycolate. [e]Reaction with phenyl glyoxal, product is ethyl mandelate. [f]Snβ in entries 12 and 13 is classic hydrothermal Snβ.

Recently, it was suggested that addition of Brønsted acid sites to a Lewis acid material led to a significant increase in ELA formation rate,[8e] suggesting that dehydration determines the reaction rate. This suggestion was corroborated by a kinetic study of Heeres et al., showing a higher activation energy for dehydration of DHA, compared to lactic acid from PAL formation, viz., respectively 93 ± 3 kJ mol^{-1} and 58 ± 14 kJ mol^{-1}.[48a] Scheme 2 summarizes the most important reactions involved in the reaction network. Note that a high rate (productivity, expressed in $g_{ELA}\cdot kg_{catalyst}^{-1}\cdot h^{-1}$) and high selectivity may only be achieved with a good balance of the Lewis and Brønsted acid sites.

Before studying the entire cascade reaction of DHA into ELA in one-pot, we decided to first probe the Lewis acid activities of the Sn/pDeAlβ zeolites in the PAL to ELA conversion in ethanol, because this single reaction only involves the Lewis acid-catalyzed hydride shift. Snβ, commercial Alβ zeolite, and Sn-free partially dealuminated β zeolite were all used as references. Results of the initial catalytic activities of the different Sn/pDeAlβ zeolite materials are tabulated in Table 2. The initial rates of all tested Sn-containing zeolites were very similar, in agreement with their Sn^{IV} content, with perhaps a slightly higher catalytic activity for the Al^{III}-rich zeolites. In addition, very low conversion rates were found for the Sn-free zeolites (Table 2, entries 1 and 2), pointing to the importance of Lewis acidity, originating from Sn^{IV}. Despite the different synthesis methods, a similar activity for hydrothermal versus Sn/pDeAlβ materials (Table 2, entry 3 vs 4−8) is found, indicating that the here presented postsynthesis procedure is a valuable alternative for the traditional synthesis method. A higher Sn content (Table 2, entry 9) results in a higher productivity, as can be expected due to the elevated Lewis acidity of this sample. Yet, due to the presence of nonframework SnO_2 species, as was evidenced with UV−vis, a lower turnover frequency was observed. Selectivity toward ELA was always higher than 99%, indicating the very limited formation of PADA and thus the absence of too strong Brønsted acidity in the zeolite samples. Next to PAL (or methyl glyoxal), the conversion of glyoxal and phenylglyoxal to their respective glycolates were also attempted (Table 2, entries 10 to 13, Scheme 3). These acids have relevant applications in pharmaceutics and as chiral chemicals as well as building blocks in polyesters.[49] Glyoxal was converted rapidly, but the selectivity was somewhat lower due to a very competitive acetalization; a high selectivity to ethyl mandelate was observed with phenyl glyoxal, although its conversion rate was significantly lower. Quantitative conversion of phenylglyoxal to the corresponding ethyl ester of mandelic acid was reached after 6 h, whereas only 2 h are required to quantitatively convert PAL to ELA. A competitive test with homogeneous $SnCl_4\cdot 5H_2O$ between equimolair quantities of glyoxal and phenyl glyoxal showed nevertheless a higher rate of formation of ethyl mandelate than ethyl glycolate (2.01 and 0.98 $mmol\cdot h^{-1}$ respectively). This reactivity difference between homo- and heterogeneous catalysis suggests a confined space around the active site or a diffusion restriction inside the zeolite. Catalytic results of these reactions with the hydrothermal Snβ resulted in a yield of ethyl glycolate similar to this of Sn/pDeAlβ, whereas the yield of ethyl mandelate was significantly lower. This difference in reactivity of the two heterogeneous catalysts is likely caused by their respectively different crystal sizes. The crystal size of a catalyst can affect the observed rate as the interior of large crystals is often not fully available to catalysis due to pore diffusion limitations, in particular when considering bulky substrates.[50] The lower ethyl mandelate yield of hydrothermal Snβ is likely caused by these diffusional restrictions (crystal size: 1000−1500 nm (SEM see Figure S3),[4a] in comparison with 10−30 nm[26] for Sn/pDeAlβ), whereas no such limitation appears for the smaller ethyl glycolate (Table 2, entries 10 vs 12 and 11 vs 13).

Scheme 3. Reaction Scheme of the Lewis Acid-Catalyzed Hydride Shift of Glyoxal (R = H), Pyruvic Aldehyde (Or Methyl Glyoxal, R = CH_3), and Phenyl Glyoxal (R = Ph) to Ethyl Glycolate, Ethyl Lactate, and Ethyl Mandelate, Respectively, Upon Reaction with Ethanol in the Presence of Sn/pDeAlβ

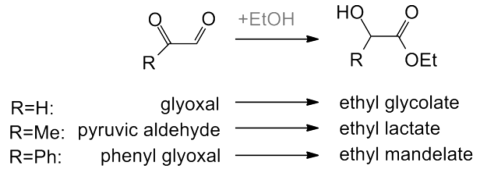

DOI: 10.1021/cs501388e
ACS Catal. 2015, 5, 928−940

Table 3. Catalytic Results of a Reaction with DHA[a]

entry	sample	initial conversion[b] %	initial ELA yield[b] %	productivity[b] $g_{ELA}\cdot kg_{catalyst}^{-1}\cdot h^{-1}$	TOF Sn[b] $mol_{ELA}\cdot mol_{Sn}^{-1}\cdot h^{-1}$	final yield/selectivity[c] %
1	Alβ	62	1	37	\	\
2	7.2pDeAlβ	25	<1	11	\	\
3	Snβ[d]	43	37	1131	72	98
4	Sn/14.4pDeAlβ	53	42	1285	78	96
5	Sn/7.2pDeAlβ	76	53	1621	103	94
6	Sn/3.6pDeAlβ	82	58	1774	112	94
7	Sn/2.88pDeAlβ	82	56	1713	118	90
8	Sn/1.44pDeAlβ	83	51	1560	103	84
9	2×Sn/2.16pDeAlβ	82	69	2111	59	92
10	2×Sn/1.8pDeAlβ	83	69	2113	57	93
11	Snβ[d] + 3.6pDeAlβ	72	40	1224	77	55

[a]Catalyst (75 mg) was added to 1 mmol of DHA in ethanol. The reaction was conducted at 363 K, and samples were taken at regular time intervals. [b]Based on sample after 30 min of reaction. [c]Final yield and selectivity after 7.5 h. [d]Snβ in entries 3 and 11 is classic hydrothermal Snβ.

A second series of catalytic experiments was carried out, focusing on the one-pot cascade DHA to ELA conversion in ethanol, which allowed us to investigate the influence of the presence of Brønsted acidity on this reaction. The catalytic results are displayed in Table 3 and plotted in Figure 7 as initial formation rate of ELA (in $M_{ELA}\cdot h^{-1}$, sampled after 0.5 h) versus the Al_{IVb} content per catalyst weight (in wt %), representing the genuine Brønsted acidity of the materials. In line with our hypothesis, the initial conversion rate is proportional with the Brønsted acidity, at least up to a value of 0.23 wt % Al_{IVb} (Table 3, entries 4−6). Because their Lewis acid activity is comparable, as demonstrated above, the impact on the conversion of DHA is purely related to the action of the Brønsted acid sites, responsible for facilitating the rate determining dehydration of DHA into PAL. On top of the initial reaction rate of Al-free Snβ (15 $M_{ELA}\cdot h^{-1}$), a gain of 0.14 $M_{ELA}\cdot h^{-1}$ per μmol Al_{IVb} was found (slope of dotted line in Figure 7). A rise above 0.23 wt % Al_{IVb} exhibits a sudden steady state in conversion rate (Table 3, entries 6−8), corresponding to a maximum ELA productivity of 1774 $g\cdot kg_{catalyst}^{-1}\cdot h^{-1}$, which is about 50% higher than for the hydrothermal Al-free Snβ. At this point, Sn sites perform at maximum capacity, showing a TOF of 118 h^{-1} at 363 K.

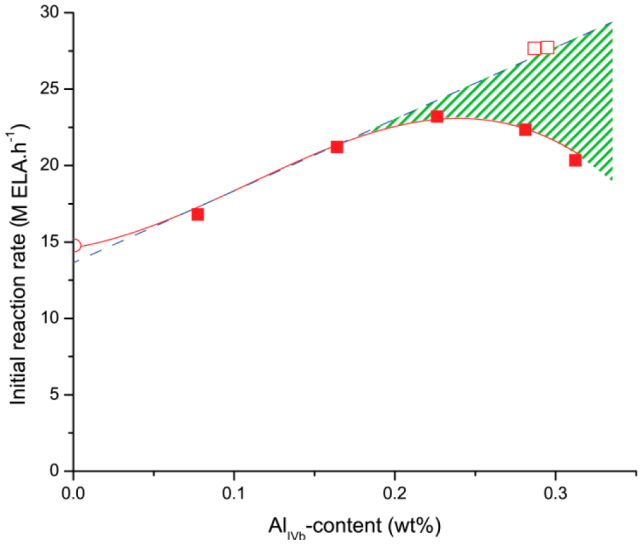

Figure 7. Initial ELA formation rate, expressed as M $ELA\cdot h^{-1}$ in function of Al_{IVb} content. Hydrothermally synthesized Snβ is depicted as a red hollow dot on the left, Sn/pDeAlβ materials (with a Sn content of 1.6 wt %) are depicted as red squares. The full red line is a guide to the eye, the dashed blue line indicates the linear correlation between reaction rate and Al_{IVb} content. The green hatched area between full and dotted line indicates the loss in reaction rate due to insufficient Sn content (hydride shift activity too low). Samples with an elevated Sn content (2×Sn/pDeAlβ, with about 3.6 wt % Sn) are shown as red hollow squares.

To demonstrate the different kinetics between an Al-free and an Al-containing Snβ-zeolite, a product distribution as a function of time for both materials is shown in Figure 8. In the initial course of the reaction a higher conversion of DHA, together with an elevated concentration of PAL and PAEA was detected for Al-containing samples. Yet, near reaction completion, all of these intermediate products are converted into ELA, leading to a final yield of 94%. Next to PAL, PAEA,

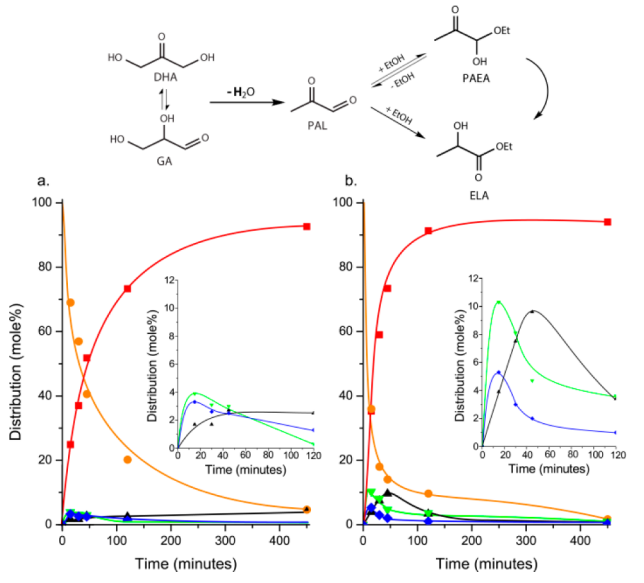

Figure 8. Distribution of DHA (orange dot), ELA (red square), GA (blue diamond), PAL (green down triangle), and PAEA (black up triangle) in function of time for the reaction of DHA to ELA in the presence of (a) hydrothermal Snβ and (b) Sn/3.6pDeAlβ. The inset shows more details for GA, PAL, and PAEA for the first 2 h of the reaction. Lines are guides for the eye. The proposed reaction scheme is shown on top.

DOI: 10.1021/cs501388e
ACS Catal. 2015, 5, 928−940

and ELA, other products were detected in the initial reaction medium. HPLC analysis of the samples demonstrated the presence of traces of GA (glyceraldehyde, the isomerization product of DHA) and hexoses like fructose (as product of an aldol reaction between DHA and GA), mannose and to a lower extent glucose, both isomers of fructose. The presence of hexoses in the reactant mixture indicates a unique aldol activity of Sn, which was just recently confirmed in the conversion of glycolaldehyde into four-carbon α-hydroxy acids[51] and noticed as well by Holm et al.[4d] The reverse reaction (retroaldol) is encountered more often in literature.[4c,d,8e] All of these products are produced by reversible reactions, and most components are eventually converted through DHA into ELA.

With increasing Al content, the amount of PAL and PAEA in the initial reaction mixture increases, as seen in Figure 8, pointing to a change in the rate-determining step of the cascade: from the dehydration to the Lewis acid-catalyzed hydride shift to ELA. Similar to adding Brønsted acid sites to accelerate the dehydration of DHA, more Lewis acid sites should convert PAL to ELA more rapidly at this point. This behavior was confirmed by using a material containing a high amount of Brønsted acid sites, to ensure rapid DHA conversion to PAL, but also with an elevated Lewis acid site density, here 3.6 wt % instead of 1.6 wt % Sn (Table 3, entry 9 and 10). Use of this catalyst led to a record ELA productivity of 2113 g·$kg_{catalyst}^{-1}$·h^{-1}. Analysis of the product distribution in the initial state of the reaction indicated similar DHA conversion as materials with comparable Al content, once again indicating that Al is responsible for the initial dehydration reaction, yet almost no PAL was detected due to its faster conversion to ELA in the presence of a catalyst with higher Sn loading. Despite the high productivity, a slightly lower TOF per Sn site was obtained as a result of the presence of SnO_2 phases in the sample with high Sn content, as ascertained above by UV−vis DRS.

Materials with higher Al-content (>0.23 wt % Al_{IVb}) show, despite a similar DHA conversion, a lower ELA yield, caused by a drop in selectivity (Table 3, entries 7 and 8 vs 6). Because formation of typical byproducts during reaction of PAL is very limited, the drop in selectivity is caused by formation of byproducts starting from DHA. The main byproducts are ethylated gluco- and fructosides (detected with GC and GCMS), which are the result of the Brønsted acid-catalyzed ethylation of glucose and fructose. These reactions are also seen on the left side in Scheme 2. As mentioned before, formation of hexoses occurs for all materials, but the formation of ethylated sugars is proportional to the amount of Brønsted acid sites present in the materials. Nonethylated sugars simply undergo the reverse Sn-catalyzed retro-aldol reaction to reform DHA and GA, but the nonreducing ethylated products are unreactive for retro-aldol reactions, causing the drop in selectivity. Another significant product was 1,1-diethoxyethane formed by a Brønsted acid addition of two molecules ethanol and acetaldehyde, which can be formed by a Sn-catalyzed Meerwein−Ponndorf−Verley (MPV) hydride shift between ethanol and a ketone substrate.[52] This ketone substrate can be DHA, PAL, or acetalized products of PAL. Snβ is a known catalyst for MPV reactions.[7,53]

The data clearly show the existence of a sensitive kinetic balance between Lewis and Brønsted acid sites. An optimal atomic Sn/Al_{IVb} ratio of 2.1 was thus deduced from the catalytic data to attain fast and selective production of ELA from DHA. A lower ratio causes a drop in selectivity, although a higher ratio lacks dehydration activity. Practically, the absolute amount of active Lewis acid Sn^{IV} sites, which can be introduced into the framework, is limited by our grafting method (and the capacity of heteroatom substitution in the BEA framework[54]) to about 3 wt % Sn. Higher amounts of Sn causes formation of nonactive extraframework Sn species.

To further demonstrate the distinctive roles of Sn^{IV} and Al^{III} in the partially dealuminated Sn-grafted materials, both an Al-free Snβ (hydrothermal Snβ) and a Sn-free Alβ (7.2DeAlβ) were tested in the conversion of an equimolar mixture of DHA and PAL. Results of these tests are displayed in Figure 9. In order to exclude the effect of the reversible isomerization of DHA to GA, the graph shows the sum of these two isomers. A significant difference in substrate preference is evident from the results. In the presence of both DHA and PAL, the Sn-containing material selectively converts PAL into ELA and leaves DHA almost untouched. The Al-containing material shows a significant conversion of DHA, whereas no significant increase or decrease in PAL concentration is found. This observation demonstrates that PAL formation from DHA and conversion to PAEA occur at similar rates, which explains the constant PAL concentration. Because no formation of ELA observed in the Al-only sample, conversion of PAEA to ELA (hydride shift) is not catalyzed by Al^{III} at 363 K. These results confirm that indeed Al is responsible for the conversion of DHA, and Sn is responsible for the hydride shift needed to form ELA.

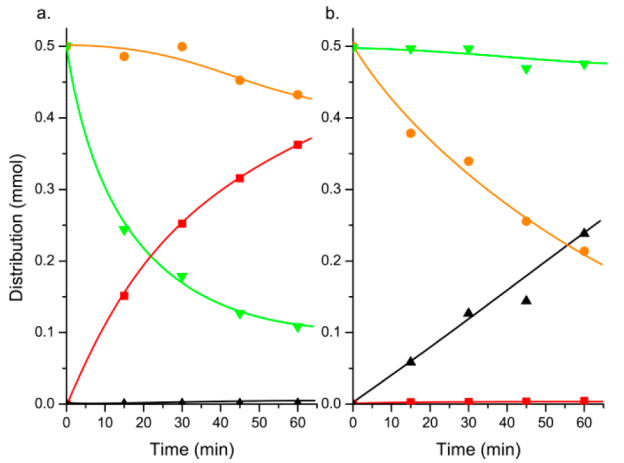

Figure 9. Plot of concentration of DHA + GA (orange dots), PAL (green down triangle), ELA (red squares), PAEA (black up triangles) in function of time for the reaction with an equimolar PAL and DHA mixture in the presence of (a) Snβ, (b) 7.2pDeAlβ. Catalyst (25 mg) was mixed with 0.5 mmol of DHA and PAL each in 5 mL of ethanol, and the reaction was conducted at 363 K. Lines are guides for the eye.

In order to check the need for proximity of both catalytic sites in one zeolite, a physical mixture of a Sn-only material (Snβ) and an Al-only material (3.6pDeAlβ) was tested. The productivity of the physical mixture only reached 69% of the productivity of a material containing the equal amounts of Brønsted and Lewis acid sites in one zeolite, viz., Sn/3.6pDeAlβ (Table 3, entry 6). The catalytic result is only marginally higher than a Al-free Snβ material. This comparison clearly underlines that the proximity of both types of acid sites is key in order to create a highly productive catalyst.

To verify the stability of the catalyst, three consecutive reactions were run with the same catalyst material. Between runs the catalyst was dried at 333 K and weighed before the

DOI: 10.1021/cs501388e
ACS Catal. 2015, 5, 928−940

next run, in order to maintain a constant substrate-to-catalyst ratio. Results of this reuse study are shown in Figure 10. The

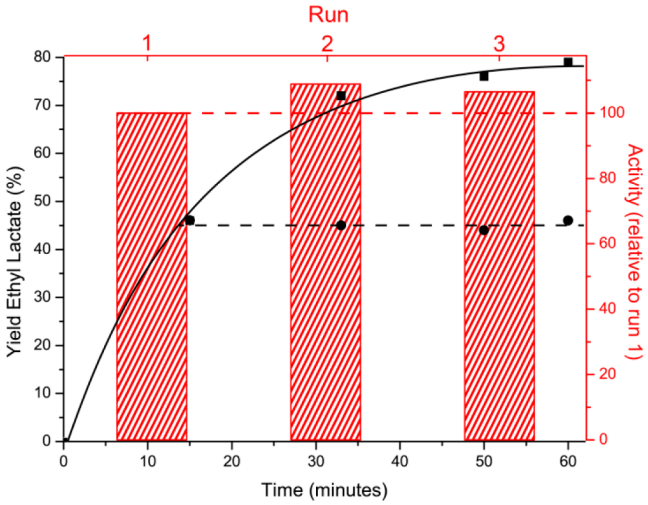

Figure 10. Results of hot filtration test (left-hand side and bottom black axis, black data points) and reuse study (right-hand side and top red axis, red hatched blocks) with Sn/3,6pDeAlβ. For the filtration test, squares and full line show the data from the reaction with the heterogeneous catalyst. Dots and the striped line show the data for the filtrate, after separating the solid catalyst after 15 min of reaction under standard conditions. The results of the reuse study show the activity (initial productivity) of each run relative to the first run (the striped red line indicates 100% activity of the first run). The catalyst was dried at 333 K between each run, a constant substrate-to-catalyst ratio was maintained.

catalyst proved to be perfectly reusable, as no sign of loss in catalytic activity was observed. This regeneration test demonstrates a true heterogeneous catalytic activity, which was also in line with the result of the following hot filtration test: after 15 min of reaction, half of the reaction medium was taken from the solution, the heterogeneous material was removed and the liquid was replaced in the reaction conditions and analyzed in similar ways as the heterogeneous reaction. Homogeneous Sn species are known catalysts for this conversion,[48a,55] but no further ethyl lactate formation was observed, hereby proving the truly heterogeneous nature of the presented bifunctional catalyst.

CONCLUSION

A simple procedure to obtain a β zeolite with both Lewis acidic Sn and Brønsted acidic Al sites, incorporated into the same framework, is presented. The synthesis method consists of a two-step procedure, which comprises a partial dealumination of a commercially available β zeolite and a grafting of $SnCl_4$ onto the partially dealuminated zeolite. In the first step, the level of dealumination can easily be varied to differ the amount of Al remaining in the framework by changing the acid concentration used. The amount of Sn can be modified by changes in the concentration of the $SnCl_4$ solution during the subsequent grafting procedure. Characterization of the materials showed the presence of Brønsted acidic tetrahedral Al and Lewis acidic Sn^{IV} in the zeolite framework. Sn seems to be present in the material in a similar way as in hydrothermally synthesized Snβ material; only Sn^{4+} was detected (^{119}Sn Möβbauer, XPS), no significant level of SnO_2 was observed (UV−vis, XRD, ^{119}Sn MAS NMR, ^{119}Sn Möβbauer), and spectroscopic features of the closed Sn site were found (^{119}Sn MAS NMR, FTIR of adsorbed deuterated acetonitrile).

The catalytic activity of the bifunctional material was tested in the conversion of DHA into ELA. Materials with Al clearly showed a faster formation of ELA in comparison with Al-free materials with similar Sn content. This behavior is due to a more efficient conversion of DHA, caused by a fast Brønsted acid-catalyzed dehydration reaction. By catalyzing the reaction of DHA to PAL with Al, Sn can be optimally used to convert PAL into ELA, resulting in a material with a productivity of 1774 $g_{ELA}{\cdot}kg_{catalyst}^{-1}{\cdot}h^{-1}$ and TOF per Sn site of 118 mol ELA.mol $Sn^{-1}{\cdot}h^{-1}$. The ideal atomic ratios of Sn to Al for fast and selective DHA conversion to ELA is about 2. Elevation of the Al and Sn content (with Sn: Al ∼2, with 3.6 wt % Sn) resulted in even higher productivities (2113 $g_{ELA}{\cdot}kg_{catalyst}^{-1}{\cdot}h^{-1}$) due to faster PAL-to-ELA formation. Higher Sn contents are unproductive due to additional formation of inactive SnO_2 phases. Note that although about 3 wt % grafted Sn^{IV} seems the ideal content of Sn to convert DHA to PAL in alcohol, we earlier found an ideal 0.5 wt % Sn^{IV} for the isomerization of sugars in water using the same synthesis protocol.[4a] Selectivity to ELA is always larger than 90%, only when high concentrations of Al are present, a drop in selectivity due to side reactions is observed. Finally, it was proven that the proximity of both Brønsted and Lewis acid sites in one framework is a prerequisite to attain a beneficial and optimal catalytic tandem effect. Additional tests proved the full recyclability of the catalyst and its truly heterogeneous nature.

ASSOCIATED CONTENT

Supporting Information

The following file is available free of charge on the ACS Publications website at DOI: 10.1021/cs501388e.

Results of X-ray diffraction, SEM, ^{119}Sn−Möβbauer, d_3-acetonitrile probed FTIR, DR UV−vis spectroscopy, and ^{29}Si and ^{27}Al MAS NMR analyses, as well as plots of Al content versus measured Brønsted acidity and SnO_2 detection limit determination for ^{119}Sn Möβbauer, ^{119}Sn MAS NMR, X-ray diffraction, and DR UV−vis (PDF)

AUTHOR INFORMATION

Corresponding Author

*E-mail: Bert.Sels@biw.kuleuven.be.

Notes

The authors declare no competing financial interest.

ACKNOWLEDGMENTS

Prof. Bart Blanpain is gratefully thanked for the EPMA measurements Hercules Foundation (project ZW09-09) is acknowledged for the funding of the JEOL JXA-8530F EPMA. J.D. thanks Methusalem CASAS for funding, and M.D. acknowledges the Research Foundation − Flanders (FWO) for postdoctoral funding and the Belgian American Educational Foundation (BAEF) for his honorary fellowship. The Belgian government is acknowledged for financial support through IAP funding (Belspo).

REFERENCES

(1) (a) Makshina, E. V.; Dusselier, M.; Janssens, W.; Degreve, J.; Jacobs, P. A.; Sels, B. F. *Chem. Soc. Rev.* **2014**, *43*, 7917−7953. (b) Besson, M.; Gallezot, P.; Pinel, C. *Chem. Rev.* **2013**, *114*, 1827−

DOI: 10.1021/cs501388e
ACS Catal. 2015, 5, 928−940

1870. (c) Van De Vyver, S.; Geboers, J.; Jacobs, P. A.; Sels, B. F. *ChemCatChem.* **2011**, *3*, 82−94. (d) Lange, J.-P. *Biofuel. Bioprod. Bior.* **2007**, *1*, 39−48. (e) Verendel, J. J.; Church, T. L.; Andersson, P. G. *Synthesis* **2011**, *11*, 1649−1677. (f) Mohan, D.; Pittman, C. U.; Steele, P. H. *Energy Fuels* **2006**, *20*, 848−889. (g) Sutton, D.; Kelleher, B.; Ross, J. R. H. *Fuel Process. Technol.* **2001**, *73*, 155−173. (h) Taarning, E.; Osmundsen, C. M.; Yang, X. B.; Voss, B.; Andersen, S. I.; Christensen, C. H. *Energy Environ. Sci.* **2011**, *4*, 793−804. (i) ten Dam, J.; Hanefeld, U. *ChemSusChem* **2011**, *4*, 1017−1034. (j) Gallezot, P. *Catal. Today* **2007**, *121*, 76−91. (k) Werpy, T.; Petersen, G. *Top Value Added Chemicals From Biomass*; U.S. Department of Energy, 2004;. (l) Moliner, M. *Dalton Trans.* **2014**, *43*, 4197−4208.

(2) (a) Ooms, R.; Dusselier, M.; Geboers, J. A.; Op de Beeck, B.; Verhaeven, R.; Gobechiya, E.; Martens, J. A.; Redl, A.; Sels, B. F. *Green Chem.* **2014**, *16*, 695−707. (b) Op de Beeck, B.; Dusselier, M.; Geboers, J.; Holsbeek, J.; Morre, E.; Oswald, S.; Giebeler, L.; Sels, B. F. *Energy Environ. Sci.* **2015**, *8*, 230−240. (c) Op de Beeck, B.; Geboers, J.; Van de Vyver, S.; Van Lishout, J.; Snelders, J.; Huijgen, W. J. J.; Courtin, C. M.; Jacobs, P. A.; Sels, B. F. *ChemSusChem* **2013**, *6*, 199−208. (d) Dusselier, M.; Van Wouwe, P.; Dewaele, A.; Makshina, E.; Sels, B. F. *Energy Environ. Sci.* **2013**, *6*, 1415−1442. (e) Dusselier, M.; Mascal, M.; Sels, B. F. *Top. Curr. Chem.* **2014**, *353*, 1−40. (f) Bozell, J. J. *Science* **2010**, *329*, 522−523. (g) Geboers, J. A.; Van de Vyver, S.; Ooms, R.; Op de Beeck, B.; Jacobs, P. A.; Sels, B. F. *Catal. Sci. Technol.* **2011**, *1*, 714−726.

(3) (a) Van de Vyver, S.; Peng, L.; Geboers, J.; Schepers, H.; de Clippel, F.; Gommes, C. J.; Goderis, B.; Jacobs, P. A.; Sels, B. F. *Green Chem.* **2010**, *12*, 1560−1563. (b) de Clippel, F.; Dusselier, M.; Van de Vyver, S.; Peng, L.; Jacobs, P. A.; Sels, B. F. *Green Chem.* **2013**, *15*, 1398−1430.

(4) (a) Dijkmans, J.; Gabriels, D.; Dusselier, M.; de Clippel, F.; Vanelderen, P.; Houthoofd, K.; Malfliet, A.; Pontikes, Y.; Sels, B. F. *Green Chem.* **2013**, *15*, 2777−2785. (b) Moliner, M.; Román-Leshkov, Y.; Davis, M. E. *Proc. Natl. Acad. Sci. U. S. A.* **2010**, *107*, 6164−6168. (c) Holm, M. S.; Saravanamurugan, S.; Taarning, E. *Science* **2010**, *328*, 602−605. (d) Holm, M. S.; Pagan-Torres, Y. J.; Saravanamurugan, S.; Riisager, A.; Dumesic, J. A.; Taarning, E. *Green Chem.* **2012**, *14*, 702−706. (e) Paris, C.; Moliner, M.; Corma, A. *Green Chem.* **2013**, *15*, 2101−2109.

(5) (a) Gunther, W. R.; Duong, Q.; Román-Leshkov, Y. *J. Mol. Catal. A: Chem.* **2013**, *379*, 294−302. (b) Gunther, W. R.; Wang, Y.; Ji, Y.; Michaelis, V. K.; Hunt, S. T.; Griffin, R. G.; Román-Leshkov, Y. *Nat. Commun.* **2012**, *3*, 1109−1116. (c) Bermejo-Deval, R.; Orazov, M.; Gounder, R.; Hwang, S.-J.; Davis, M. E. *ACS Catal.* **2014**, *4*, 2288−2297.

(6) Corma, A.; Nemeth, L. T.; Renz, M.; Valencia, S. *Nature* **2001**, *412*, 423−425.

(7) Corma, A.; Domine, M. E.; Valencia, S. *J. Catal.* **2003**, *215*, 294−304.

(8) (a) Dapsens, P. Y.; Mondelli, C.; Jagielski, J.; Hauert, R.; Perez-Ramirez, J. *Catal. Sci. Technol.* **2014**, *4*, 2302−2311. (b) Witvrouwen, T.; Dijkmans, J.; Paulussen, S.; Sels, B. *Plasma Processes Polym.* **2014**, *11*, 464−471. (c) Li, L.; Collard, X.; Bertrand, A.; Sels, B. F.; Pescarmona, P. P.; Aprile, C. *J. Catal.* **2014**, *314*, 56−65. (d) Osmundsen, C. M.; Holm, M. S.; Dahl, S.; Taarning, E. *Proc. R. Soc. A* **2012**, *468*, 2000−2016. (e) de Clippel, F.; Dusselier, M.; Van Rompaey, R.; Vanelderen, P.; Dijkmans, J.; Makshina, E.; Giebeler, L.; Oswald, S.; Baron, G. V.; Denayer, J. F. M.; Pescarmona, P. P.; Jacobs, P. A.; Sels, B. F. *J. Am. Chem. Soc.* **2012**, *134*, 10089−10101. (f) Li, L.; Stroobants, C.; Lin, K.; Jacobs, P. A.; Sels, B. F.; Pescarmona, P. P. *Green Chem.* **2011**, *13*, 1175−1181. (g) Witvrouwen, T.; Dijkmans, J.; Paulussen, S.; Sels, B. *J. Energy Chem.* **2013**, *22*, 451−458.

(9) Gounder, R.; Davis, M. E. *J. Catal.* **2013**, *308*, 176−188.

(10) Román-Leshkov, Y.; Moliner, M.; Labinger, J. A.; Davis, M. E. *Angew. Chem.-Int. Ed.* **2010**, *49*, 8954−8957.

(11) Naber, J. E.; de Jong, K. P.; Stork, W. H. J.; Kuipers, H. P. C. E.; Post, M. F. M. *Stud. Surf. Sci. Catal.* **1994**, *84*, 2197−2219.

(12) Kuster, B. F. M. *Starch-Starke* **1990**, *42*, 314−321.

(13) Nikolla, E.; Román-Leshkov, Y.; Moliner, M.; Davis, M. E. *ACS Catal.* **2011**, *1*, 408−410.

(14) Lew, C. M.; Rajabbeigi, N.; Tsapatsis, M. *Ind. Eng. Chem. Res.* **2012**, *51*, 5364−5366.

(15) Choudhary, V.; Pinar, A. B.; Sandler, S. I.; Vlachos, D. G.; Lobo, R. F. *ACS Catal.* **2011**, *1*, 1724−1728.

(16) Bui, L.; Luo, H.; Gunther, W. R.; Román-Leshkov, Y. *Angew. Chem., Int. Ed.* **2013**, *52*, 8022−8025.

(17) Schwartz, T. J.; Goodman, S. M.; Osmundsen, C. M.; Taarning, E.; Mozuch, M. D.; Gaskell, J.; Cullen, D.; Kersten, P. J.; Dumesic, J. A. *ACS Catal.* **2013**, *3*, 2689−2693.

(18) (a) Mal, N. K.; Ramaswamy, A. V. *Chem. Commun. (Cambridge)* **1997**, 425−426. (b) UOP LLC. Valencia, S. V.; Corma, A. C. U.S. Patent No. US005968473A, October 19, 1999.

(19) van Grieken, R.; Martos, C.; Sánchez-Sánchez, M.; Serrano, D. P.; Melero, J. A.; Iglesias, J.; Cubero, A. G. *Microporous Mesoporous Mater.* **2009**, *119*, 176−185.

(20) (a) Li, P.; Liu, G.; Wu, H.; Liu, Y.; Jiang, J.-g.; Wu, P. *J. Phys. Chem. C* **2011**, *115*, 3663−3670. (b) Kang, Z.; Liu, H. o.; Zhang, X. *Chin. J. Catal.* **2012**, *33*, 898−904. (c) Hammond, C.; Conrad, S.; Hermans, I. *Angew. Chem.-Int. Ed.* **2012**, *51*, 11736−11739. (d) Tang, B.; Dai, W.; Wu, G.; Guan, N.; Li, L.; Hunger, M. *ACS Catal.* **2014**, *4*, 2801−2810.

(21) Nesterenko, N. S.; Thibault-Starzyk, F.; Montouilliout, V.; Yushchenko, V. V.; Fernandez, C.; Gilson, J. P.; Fajula, F.; Ivanova, I. I. *Kinet. Catal.* **2006**, *47*, 40−48.

(22) Chaudhari, K.; Das, T. K.; Rajmohanan, P. R.; Lazar, K.; Sivasanker, S.; Chandwadkar, A. J. *J. Catal.* **1999**, *183*, 281−291.

(23) (a) Dusselier, M.; Wouwe, P. v.; Clippel, F. d.; Dijkmans, J.; Gammon, D. W.; Sels, B. F. *ChemCatChem.* **2012**, *5*, 569−575. (b) Dusselier, M.; Sels, B. F. *Top. Curr. Chem.* **2014**, *353*, 85−125. (c) Garlotta, D. *J. Polym. Environ.* **2001**, *9*, 63−84. (d) Wang, Y.; Deng, W.; Wang, B.; Zhang, Q.; Wan, X.; Tang, Z.; Wang, Y.; Zhu, C.; Cao, Z.; Wang, G.; Wan, H. *Nat. Commun.* **2013**, *4*, 2141−2147. (e) Chambon, F.; Rataboul, F.; Pinel, C.; Cabiac, A.; Guillon, E.; Essayem, N. *Appl. Catal., B* **2011**, *102*, 171−181.

(24) (a) Lami, E. B.; Fajula, F.; Anglerot, D.; Des Courieres, T. *Microporous Mater.* **1993**, *1*, 237−245. (b) Omegna, A.; Vasic, M.; Anton van Bokhoven, J.; Pirngruber, G.; Prins, R. *Phys. Chem. Chem. Phys.* **2004**, *6*, 447−452.

(25) Casagrande, M.; Moretti, E.; Storaro, L.; Lenarda, M.; Gersich, J.; Stievano, L.; Wagner, F. E. *Microporous Mesoporous Mater.* **2006**, *91*, 261−267.

(26) Demuynck, A. L. W.; Levecque, P.; Kidane, A.; Gammon, D. W.; Sickle, E.; Jacobs, P. A.; De Vos, D. E.; Sels, B. F. *Adv. Synth. Catal.* **2010**, *352*, 3419−3430.

(27) Flinn, P. A. *Mössbauer Isomer Shifts*; North-Holland Publishing company: Amsterdam, 1978; pp 601−604.

(28) Fejes, P.; Nagy, J. B.; Kovács, K.; Vankó, G. *Appl. Catal., A* **1996**, *145*, 155−184.

(29) Bermejo-Deval, R.; Gounder, R.; Davis, M. E. *ACS Catal.* **2012**, *2*, 2705−2713.

(30) Gunther, W. R.; Michaelis, V. K.; Caporini, M. A.; Griffin, R. G.; Román-Leshkov, Y. *J. Am. Chem. Soc.* **2014**, *136*, 6219−6222.

(31) Wolf, P.; Valla, M.; Rossini, A. J.; Comas-Vives, A.; Núñez-Zarur, F.; Malaman, B.; Lesage, A.; Emsley, L.; Copéret, C.; Hermans, I. *Angew. Chem., Int. Ed.* **2014**, *53*, 10179−10183.

(32) Renz, M.; Blasco, T.; Corma, A.; Fornes, V.; Jensen, R.; Nemeth, L. *Chem.—Eur. J.* **2002**, *8*, 4708−4717.

(33) (a) Boronat, M.; Concepcion, P.; Corma, A.; Renz, M.; Valencia, S. *J. Catal.* **2005**, *234*, 111−118. (b) Roy, S.; Bakhmutsky, K.; Mahmoud, E.; Lobo, R. F.; Gorte, R. J. *ACS Catal.* **2013**, *3*, 573−580.

(34) Jänchen, J.; Busio, M.; Hintze, M.; Stach, H.; van Hooff, J. H. C. *Stud. Surf. Sci. Catal.* **1997**, *105*, 1731−1738.

(35) Vimont, A.; Thibault-Starzyk, F.; Lavalley, J. C. *J. Phys. Chem. B* **1999**, *104*, 286−291.

(36) Zecchina, A.; Bordiga, S.; Spoto, G.; Marchese, L.; Petrini, G.; Leofanti, G.; Padovan, M. *J. Phys. Chem.* **1992**, *96*, 4991−4997.

DOI: 10.1021/cs501388e
ACS Catal. 2015, 5, 928−940

(37) (a) Fink, P.; Camara, B.; Welz, E.; Ty, P. *Z. Chem.* **1971**, *11*, 473−474. (b) Ertl, G.; Knözinger, H.; Schüth, F.; Weitkamp, J. *Handbook of Heterogeneous Catalysis*; Wiley-VCH: Weinheim, 2008; p 961.
(38) Penzien, J.; Abraham, A.; van Bokhoven, J. A.; Jentys, A.; Müller, T. E.; Sievers, C.; Lercher, J. A. *J. Phys. Chem. B* **2004**, *108*, 4116−4126.
(39) (a) van Bokhoven, J. A.; Koningsberger, D. C.; Kunkeler, P.; van Bekkum, H.; Kentgens, A. P. M. *J. Am. Chem. Soc.* **2000**, *122*, 12842−12847. (b) Roberge, D. M.; Hausmann, H.; Holderich, W. F. *Phys. Chem. Chem. Phys.* **2002**, *4*, 3128−3135.
(40) Vjunov, A.; Fulton, J. L.; Huthwelker, T.; Pin, S.; Mei, D.; Schenter, G. K.; Govind, N.; Camaioni, D. M.; Hu, J. Z.; Lercher, J. A. *J. Am. Chem. Soc.* **2014**, *136*, 8296−8306.
(41) (a) Emeis, C. A. *J. Catal.* **1993**, *141*, 347−354. (b) Morin, S.; Ayrault, P.; El Mouahid, S.; Gnep, N. S.; Guisnet, M. *Appl. Catal., A* **1997**, *159*, 317−331. (c) Khabtou, S.; Chevreau, T.; Lavalley, J. C. *Microporous Mater.* **1994**, *3*, 133−148.
(42) Tolborg, S.; Katerinopoulou, A.; Falcone, D. D.; Sadaba, I.; Osmundsen, C. M.; Davis, R. J.; Taarning, E.; Fristrup, P.; Holm, M. S. *J. Mater. Chem., A* **2014**, *2*, 20252−20262.
(43) Choudhary, V.; Sandler, S. I.; Vlachos, D. G. *ACS Catal.* **2012**, *2*, 2022−2028.
(44) Taarning, E.; Saravanamurugan, S.; Holm, M. S.; Xiong, J.; West, R. M.; Christensen, C. H. *ChemSusChem* **2009**, *2*, 625−627.
(45) Dusselier, M.; Van Wouwe, P.; De Smet, S.; De Clercq, R.; Verbelen, L.; Van Puyvelde, P.; Du Prez, F. E.; Sels, B. F. *ACS Catal.* **2013**, *3*, 1786−1800.
(46) Yamaguchi, S.; Motokura, K.; Sakamoto, Y.; Miyaji, A.; Baba, T. *Chem. Commun.* **2014**, *50*, 4600−4602.
(47) (a) Pereira, C. S. M.; Silva, V. M. T. M.; Rodrigues, A. E. *Green Chem.* **2011**, *13*, 2658−2671. (b) Van Wouwe, P.; Dusselier, M.; Basic, A.; Sels, B. F. *Green Chem.* **2013**, *15*, 2817−2824.
(48) (a) Rasrendra, C. B.; Fachri, B. A.; Makertihartha, I. G. B. N.; Adisasmito, S.; Heeres, H. J. *ChemSusChem* **2011**, *4*, 768−777. (b) Pescarmona, P. P.; Janssen, K. P. F.; Delaet, C.; Stroobants, C.; Houthoofd, K.; Philippaerts, A.; De Jonghe, C.; Paul, J. S.; Jacobs, P. A.; Sels, B. F. *Green Chem.* **2010**, *12*, 1083−1089.
(49) (a) Wang, Z.; Jiang, Y.; Baiker, A.; Huang, J. *ACS Catal.* **2013**, *3*, 1573−1577. (b) Dapsens, P. Y.; Mondelli, C.; Kusema, B. T.; Verel, R.; Perez-Ramirez, J. *Green Chem.* **2014**, *16*, 1176−1186.
(50) van der Pol, A. J. H. P.; Verduyn, A. J.; van Hooff, J. H. C. *Appl. Catal., A* **1992**, *92*, 113−130.
(51) Dusselier, M.; Van Wouwe, P.; De Smet, S.; De Clercq, R.; Verbelen, L.; Van Puyvelde, P.; Du Prez, F. E.; Sels, B. F. *ACS Catal.* **2013**, *3*, 1786−1800.
(52) (a) Meerwein, H.; Schmidt, R. *Justus Liebigs Ann. Chem.* **1925**, *444*, 221−238. (b) Ponndorf, W. *Angew. Chem.* **1926**, *39*, 138−143. (c) Verley, A. *Bull. Soc. Chim. Fr.* **1925**, *37*, 537.
(53) (a) Corma, A.; Domine, M. E.; Nemeth, L.; Valencia, S. *J. Am. Chem. Soc.* **2002**, *124*, 3194−3195. (b) Boronat, M.; Corma, A.; Renz, M. *J. Phys. Chem. B* **2006**, *110*, 21168−21174.
(54) Shetty, S.; Pal, S.; Kanhere, D. G.; Goursot, A. *Chem.—Eur. J.* **2006**, *12*, 518−523.
(55) Hayashi, Y.; Sasaki, Y. *Chem. Commun.* **2005**, 2716−2718.

DOI: 10.1021/cs501388e
ACS Catal. 2015, 5, 928−940